

## 2db numerical simulations of incompressible environmental flows

Leon Matos Ribeiro de Lima<sup>1</sup>, Norberto Mangiavacchi<sup>1</sup>, José Pontes<sup>2</sup>  
and Cássio Botelho Pereira Soares<sup>3</sup>

Manuscript received on January 11, 2011 / accepted on December 10, 2011

### ABSTRACT

Many impacts associated to environmental flows strongly depend on the depth of the aquatic body, such as thermal and hydraulic stratifications, which can lead to formation of layers with different concentrations of oxygen and nutrients. To simulate such problems numerically, for many applications, the most efficient approach is a laterally averaged model (2db), rather than a 3d approach. This paper presents a laterally averaged Finite Element model applied to environmental flow simulations and temperature/pollutant transport to predict effects of stratification, in the context of hydroelectric reservoirs. The work includes the development of computational tools for terrain data manipulation and mesh generation. A validation procedure against experimental results is shown, as well as a numerical simulation of an environmental flow.

**Keywords:** laterally averaged 2d model, thermal stratification, environmental flows, Finite Element Method.

### 1 INTRODUCTION

Intense industrialization of emerging countries has placed an increasing burden on the environment [6], and our awareness on the relationship between pollutant transport and environment impact has enhanced the role played by prediction methods on this class of problem. Many environmental phenomena related to water resources are strongly dependent on the depth of the aquatic body, such as thermal and/or hydraulic stratification and organic material transport. Changes of the main parameters associated to these problems along the reservoir depth are much more significant than the changes along parallel to the surface.

Concerning stratified flows, aquatic bodies with low velocity flows are common to several environments, such as hydroelectric reservoirs, water cooling pools and lakes, and have favorable conditions for the formation of thermal stratification. Addition-

ally, thermal stratification is influenced by other variables, and can sometimes be broken, causing many perturbations in local ecosystems. This may result in the accumulation of poor quality water in the lower layers, many times in anaerobic conditions, configuring a region of low oxygen concentrations and high acidity. Wind and low temperatures at the surface, for instance, may brake the stratification, pushing the bad quality water to the top, causing negative ecological impacts that influence local fauna. Many times, specially in deep water reservoirs, the stratification acts as a barrier against the water from the bottom to rise toward the surface, being a favorable factor to water pollution control.

#### 1.1 Modeling

Models for predictions of environmental impacts play an increasing role on the study and control of ecological systems wealth.

Correspondence to: Leon Matos Ribeiro de Lima – E-mail: matosleon@gmail.com

<sup>1</sup>Rio de Janeiro State University, Rua Fonseca Teles, 121, São Cristóvão, 20940-200 Rio de Janeiro, RJ, Brazil.

<sup>2</sup>Federal University of Rio de Janeiro, Cidade Universitária, 20000-000 Rio de Janeiro, RJ, Brazil.

<sup>3</sup>FURNAS Centrais Elétricas, Rua Real Grandeza, 219, Botafogo, 22281-035 Rio de Janeiro, RJ, Brazil.

E-mails: norberto.mangiavacchi@gmail.com / jopontes@metalmat.ufrj.br / cassiobp@furnas.com.br

Mathematical models for water bodies like hydroelectric reservoirs can be classified taking into account the number of space dimensions, i.e. 3d, 2d, 1d and 0d. In the particular case of flows where the depth direction is considerably more relevant than the longitudinal and transverse directions, 2d approaches are often more suitable for several environmental flows than 3d models, because they provide, in many applications, predictions with the required accuracy in short processing times compared to the respective 3d simulation. In the specific case of narrow estuaries, the most appropriate 2d model is derived by integrating across the reservoir [3, 9], which leads to the laterally averaged equations of motion (2db).

This paper presents a laterally averaged Finite Element model applied to environmental flow simulations and temperature/pollutant transport to predict effects of stratification, in the context of hydroelectric reservoirs. The work includes the development of computational tools for terrain data manipulation and mesh generation. The system of equations is numerically solved by the Finite Element Method, where the velocity and pressure fields are decoupled by the discrete Projection Method. Space domain is discretized by the standard Galerkin method, and time domain is discretized by a first order semi-Lagrangian method. Computational codes have been developed under the Object Oriented Paradigm, using C++ language.

## 2 MESH GENERATION

This section described the mesh generation procedure, which starts from reading the terrain data. The terrain files can be under two different data structures: raster terrain type (a grid of equally spaced ( $x$ ,  $y$ ,  $z$ ) coordinates) or shape terrain type (a set of level curves).

In what follows, the water body will be interpreted as a hydroelectric reservoir. In order to capture the hydrodynamic and thermal processes along the reservoir depth by a two-dimensional approach the finite element mesh must be a vertical mesh, along a certain longitudinal path. The algorithm for mesh generation is designed for irregular terrain geometries combined with hydrographic maps. Topological data are obtained from a set of level curves that provides the reservoir bottom coordinates and the breadth at each point of the vertical mesh, while the hydrographic maps provides the horizontal (or longitudinal) direction. These maps contain the coordinates associated to the riverbed, where hydrodynamic effects are probably more relevant.

Figure 1 shows a top view, in the left side, of the terrain data or a selected region combined with the hydrographic map, and,

in the right side, the riverbed line (longitudinal direction). The vertical mesh – referred to as 2db mesh – will be generated over the riverbed (highlighted blue line), which provides bottom coordinates. The orange lines represent the reservoir margins and are used in the calculation of the breadth.

After gathering the necessary information, the first stage is the triangulation on the terrain data to generate the terrain mesh (not the vertical mesh yet). This step allows interpolation of terrain coordinates at any point of the reservoir, which will be useful for bottom coordinate and breadth evaluation. The second step consists on projecting the riverbed line on the reservoir lower surface. Now, vertical triangulation can be performed to assemble the vertical mesh (third step). Figures 2 to 5 illustrate the process.

Evaluation of the breadth for each point of the 2db mesh can now be performed. In the presented model, each breadth  $B_n$  associated to node  $n$  is the sum of the distance from the node to left side,  $B_n^L$ , and to the right side,  $B_n^R$ . That is,

$$B_n = B_n^L + B_n^R. \quad (1)$$

This procedure is shown in Figure 6.

## 3 MATHEMATICAL MODEL

The equations that constitute the model are obtained by laterally integrating the incompressible Navier-Stokes equations and transport equation, as follows

$$\int_B \left[ \rho \frac{D\hat{\mathbf{v}}}{Dt} - \nabla \cdot \underline{\mathbf{I}} - \rho \mathbf{g} \right] db = 0, \quad (2)$$

$$\int_B [\nabla \cdot \hat{\mathbf{v}}] db = 0, \quad (3)$$

$$\int_B \left[ \frac{D\hat{c}}{Dt} - \nabla \cdot (D \nabla \hat{c}) \right] db = 0. \quad (4)$$

In the above equations the  $d/\partial$  operator, represented by  $\nabla$ , is used as divergent and gradient operators. The velocity field is represented by  $\hat{\mathbf{v}}$  and  $\hat{c}$  is a scalar field, which can be temperature or a generic passive concentration.  $\underline{\mathbf{I}}$  is the Cauchy stress tensor,  $\rho$  is the density,  $\mathbf{g}$  represents the gravity acceleration, given by  $\mathbf{g} = g \mathbf{k}$ , where  $g$  is the modulus of gravity acceleration, and  $D$  is the diffusivity coefficient.  $W$  represents the local breadth. The three coordinate directions are denoted by  $s$  (longitudinal direction),  $z$  (vertical direction) and  $b$  (lateral direction). That is why the integration element in the above equations is  $db$ . After integrating, and taking into account that the stress tensor is

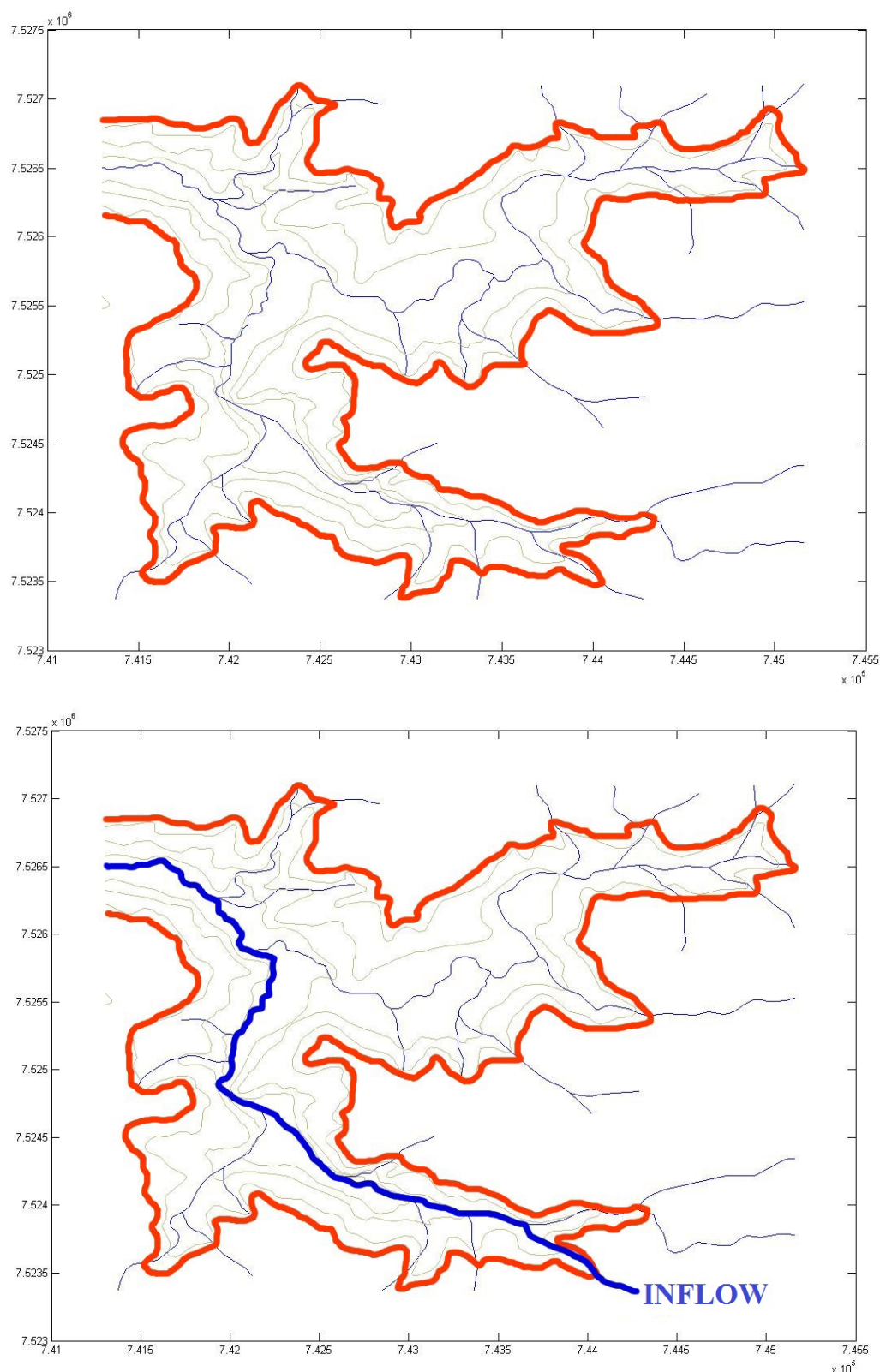
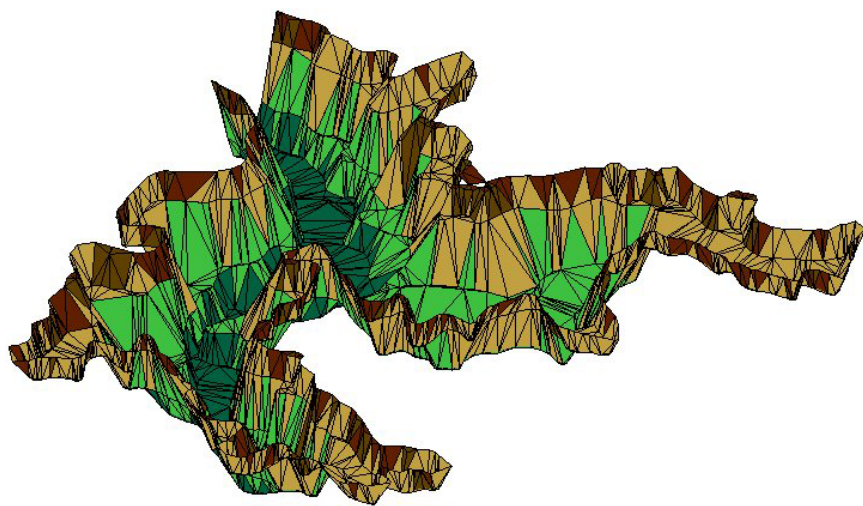
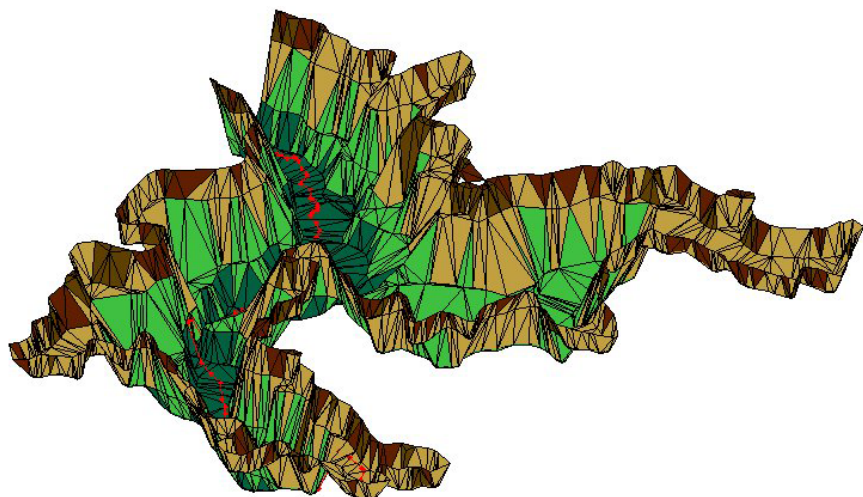


Figure 1 – Superposition of terrain and hydrographic data.



**Figure 2** – Terrain mesh.



**Figure 3** – Terrain mesh and projected riverbed.

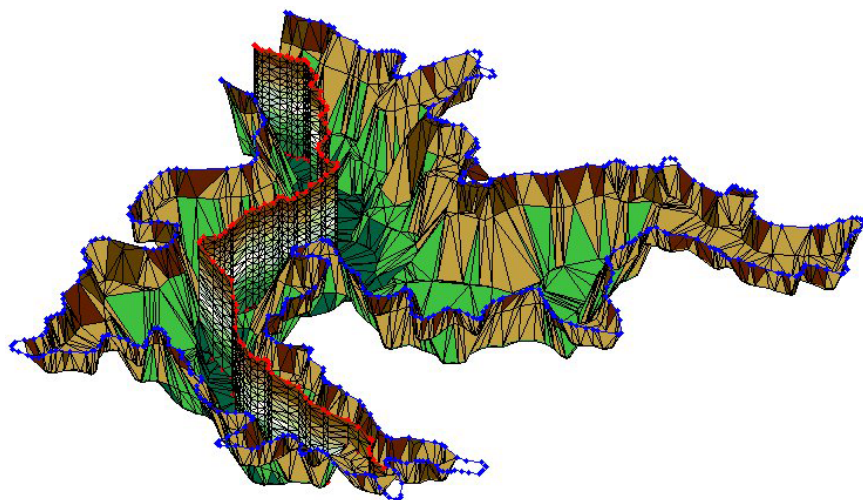


**Figure 4** – Superposition of terrain mesh and vertical mesh.

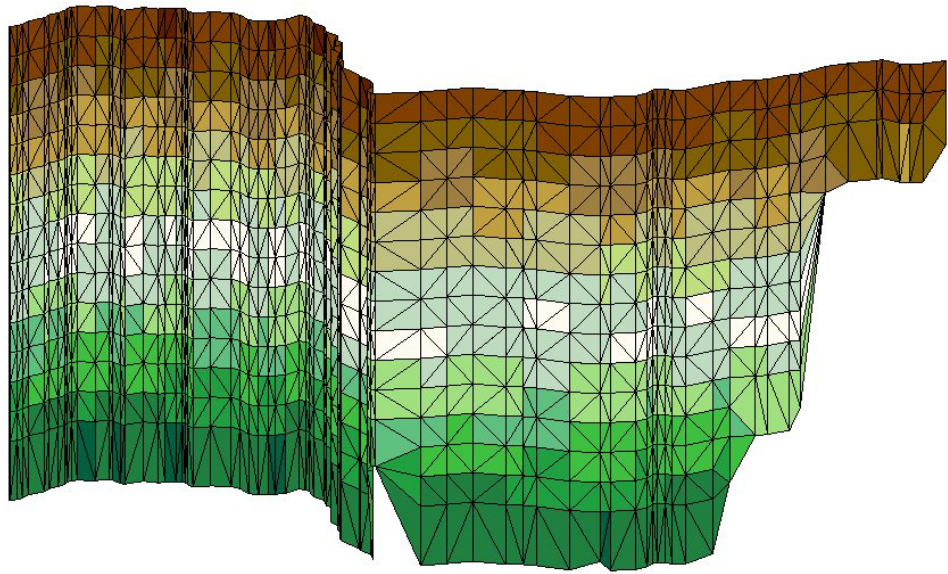


Figure 5 – Vertical mesh (2db mesh).

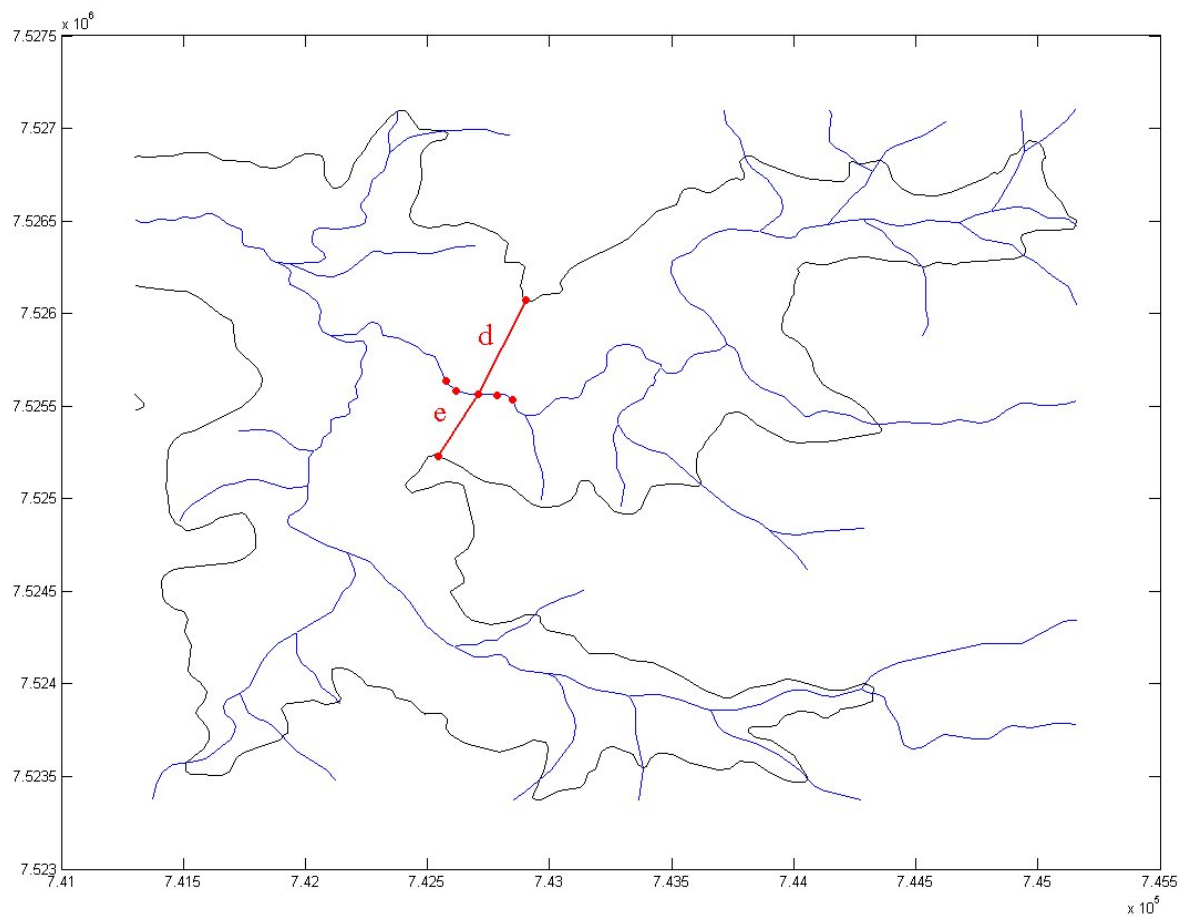


Figure 6 – Breadth calculation.

given by

$$\underline{\underline{\tau}} = \begin{bmatrix} \tau_{ss} & \tau_{sz} & \tau_{sb} \\ \tau_{zs} & \tau_{zz} & \tau_{zb} \\ \tau_{bs} & \tau_{bz} & \tau_{bb} \end{bmatrix}, \quad (5)$$

we arrive at the 2d laterally averaged equations of motion and transport [8] (in its dimensionless form, expanded in  $s$  and  $z$  coordinates):

$$\begin{aligned} \frac{\partial u}{\partial t} + u \frac{\partial u}{\partial s} + w \frac{\partial u}{\partial z} \\ = \frac{1}{\rho B Re} \left[ \frac{\partial(B\tau_{ss})}{\partial s} + \frac{\partial(B\tau_{zs})}{\partial z} \right], \end{aligned} \quad (6)$$

$$\begin{aligned} \frac{\partial w}{\partial t} + u \frac{\partial w}{\partial s} + w \frac{\partial w}{\partial z} \\ = \frac{1}{\rho B Re} \left[ \frac{\partial(B\tau_{zs})}{\partial s} + \frac{\partial(B\tau_{zz})}{\partial z} \right] + g, \end{aligned} \quad (7)$$

$$\frac{\partial(Bu)}{\partial s} + \frac{\partial(Bw)}{\partial z} = 0, \quad (8)$$

$$\begin{aligned} \frac{\partial c}{\partial t} + u \frac{\partial c}{\partial s} + w \frac{\partial c}{\partial z} \\ = \frac{1}{B Re Sc} \left[ \frac{\partial}{\partial s} \left( BD \frac{\partial c}{\partial s} \right) + \frac{\partial}{\partial z} \left( BD \frac{\partial c}{\partial z} \right) \right], \end{aligned} \quad (9)$$

where  $Re$  denotes the Reynolds number and  $Sc$  is the Schmidt number, defined by  $Sc = \nu/D$ , with  $D$  being the diffusion coefficient of the scalar,  $\nu = \mu/\rho$ , where  $\nu$  is the kinematic viscosity and  $\mu$  is the dynamic viscosity. The unknowns  $u$  and  $w$  represent the mean longitudinal and vertical velocity components, respectively. Note that some terms coming from the integration procedure were neglected. If  $\hat{\mathbf{v}} = \hat{u}\mathbf{i} + \hat{w}\mathbf{k}$  is the original velocity field and  $\mathbf{v} = u\mathbf{i} + w\mathbf{k}$  is the laterally averaged velocity field, the components of  $\mathbf{v}$  are obtained by

$$u = \frac{1}{B} \int_0^B \hat{u} db, \quad (10)$$

$$w = \frac{1}{B} \int_0^B \hat{w} db. \quad (11)$$

Similarly, the averaged concentration and pressure scalar fields are respectively given by

$$c = \frac{1}{B} \int_0^B \hat{c} db, \quad (12)$$

$$p = \frac{1}{B} \int_0^B \hat{p} db. \quad (13)$$

Considering newtonian incompressible fluid model, the stress tensor can be expressed as

$$\underline{\underline{\tau}} = -p\underline{\underline{1}} + \mu \left[ \nabla \mathbf{v} + (\nabla \mathbf{v})^T \right], \quad (14)$$

where  $p$  stands for the laterally averaged pressure field. Multiplying Eqs. 6 to 9 by  $B$ , considering Eq. 14 and taking into account that, assuming constant viscosity,  $\nabla \cdot (\nabla \mathbf{v})^T = \nabla \cdot (\nabla \cdot \mathbf{v}) = 0$ , we arrive at the 2DB momentum equations:

$$\begin{aligned} B \left( \frac{\partial u}{\partial t} + u \frac{\partial u}{\partial s} + w \frac{\partial u}{\partial z} \right) &= -\frac{1}{\rho} \frac{\partial(Bp)}{\partial x} \\ &+ \frac{\nu}{Re} \left[ \frac{\partial}{\partial s} \left( B \frac{\partial u}{\partial s} \right) + \frac{\partial}{\partial z} \left( B \frac{\partial u}{\partial z} \right) \right], \end{aligned} \quad (15)$$

$$\begin{aligned} B \left( \frac{\partial w}{\partial t} + u \frac{\partial w}{\partial s} + w \frac{\partial w}{\partial z} \right) &= -\frac{1}{\rho} \frac{\partial(Bp)}{\partial z} \\ &+ \frac{\nu}{Re} \left[ \frac{\partial}{\partial s} \left( B \frac{\partial w}{\partial s} \right) + \frac{\partial}{\partial z} \left( B \frac{\partial w}{\partial z} \right) \right] + Bg. \end{aligned} \quad (16)$$

#### 4 NUMERICAL FORMULATION

The Finite Element Method is employed to solve Eqs. 15, 16, 8 and 9. Let these equations be defined in a domain  $\Omega$  and let  $S$  be the subspace defined by

$$S = \mathcal{H}^1(\Omega)^m = \{ \mathbf{v} = (v_1, \dots, v_m) | v_i \in \mathcal{H}^1(\Omega), \forall i = 1, \dots, m \}, \quad (17)$$

where  $\mathcal{H}^1(\Omega)$  the Sobolev space of first order derivative functions square integrable over  $\Omega$ . Let  $L^2(\Omega)$  be a space of infinite dimension so that

$$L^2(\Omega) = \left\{ v : \Omega \rightarrow \mathbb{R} \mid \int_{\Omega} v^2 d\Omega < \infty \right\}. \quad (18)$$

Introducing the weight functions  $\mathbf{w}$ ,  $q$  and  $r$ , the application of Finite Element Method consists of finding solutions  $\mathbf{v} \in S$ ,  $p \in L^2$  and  $c \in L^2$  such that

$$\int_{\Omega} B \frac{D\mathbf{v}}{Dt} \cdot \mathbf{w} d\Omega + \frac{1}{\rho} \int_{\Omega} B p (\nabla \cdot \mathbf{w}) d\Omega$$

$$+ \nu \int_{\Omega} B \nabla \mathbf{v} : \nabla \mathbf{w} d\Omega - \int_{\Omega} B \mathbf{g} \cdot \mathbf{w} = 0, \quad (19)$$

$$\int_{\Omega} (\nabla \cdot \mathbf{v}) B q d\Omega = 0, \quad (20)$$

$$\int_{\Omega} B \frac{Dc}{Dt} r d\Omega + \frac{1}{Re Sc} \int_{\Omega} (BD\nabla c) \cdot \nabla r d\Omega = 0, \quad (21)$$

where  $\tau^L$  and  $\tau^R$  are left and right shear stress vectors, and the operator  $(\cdot)$  is the tensor inner product. The semi-discrete Galerkin method is employed for discretization of Eqs. 19, 20 and 21, in which time derivatives remain continue. The domain  $\Omega$  is discretized in a triangular finite element mesh. Unknowns  $u$ ,  $w$ ,  $p$  and  $c$  are approximated by

$$\hat{u}(s, z, t) \approx \sum_{N_u} N_n^u(s, z) u_n(t), \quad (22)$$

$$\hat{w}(s, z, t) \approx \sum_{N_w} N_n^w(s, z) w_n(t), \quad (23)$$

$$\hat{p}(s, z, t) \approx \sum_{N_p} N_n^p(s, z) p_n(t), \quad (24)$$

$$\hat{c}(s, z, t) \approx \sum_{N_c} N_n^c(s, z) c_n(t), \quad (25)$$

where  $N_n^u$ ,  $N_n^w$ ,  $N_n^p$  and  $N_n^c$  are the so-called shape functions. The node value of each unknown is represented by  $u_n$ ,  $w_n$ ,  $p_n$  and  $c_n$ . The number of nodes of velocity components, pressure and scalar are denoted by  $N_u$ ,  $N_w$ ,  $N_p$  and  $N_c$ . Integrations of each term over  $\Omega_e$  for all elements yield

$$\begin{aligned} M_s \dot{u} + \frac{1}{B Re} [(2K_{ss} + K_{zz}) u + K_{sz} w] \\ + \frac{g}{B} G_s B p = 0, \end{aligned} \quad (26)$$

$$\begin{aligned} M_z \dot{w} + \frac{1}{B Re} [K_{zs} u + (K_{ss} + 2K_{zz}) w] \\ + \frac{g}{B} G_z B p = 0, \end{aligned} \quad (27)$$

$$D_s u + D_z w = 0, \quad (28)$$

$$M_c \dot{c} + \frac{1}{Re Sc} (K_{ss} + K_{zz}) c = 0. \quad (29)$$

Note that the substantive derivatives of velocity components and scalar are respectively represented by  $\dot{u}$ ,  $\dot{w}$ , and  $\dot{c}$ , and are time discretized by a first order Semi-Lagrangian scheme, which allows the use of large time steps without limiting the stability, in contrast to the Eulerian framework. In principle, the choice of the time step is only limited by numerical accuracy. However, for large time steps, instabilities may appear when trajectories cross and particles “overtake” others, due to inaccuracy of the computed trajectories. If  $\Delta t$  is a finite time difference, the Semi-Lagrangian scheme approximates the convective term in a time step  $m + 1$  in the node  $n$  by

$$\frac{D \mathbf{v}_n}{Dt} \approx \frac{\mathbf{v}_n^{m+1} - \mathbf{v}_d^m}{\Delta t}, \quad (30)$$

$$\frac{D c_n}{Dt} \approx \frac{c_n^{m+1} - c_d^m}{\Delta t}, \quad (31)$$

where the subscript  $d$  (from departure) refers to the space point from which the particle came. Time and space discretization of Eqs. 26 to 28 gives rise to an algebraic linear system of the form

$$\begin{bmatrix} B & -\Delta t G \\ D & 0 \end{bmatrix} \begin{bmatrix} \mathbf{v}^{m+1} \\ p^{m+1} \end{bmatrix} = \begin{bmatrix} a_{\mathbf{v}}^{m+1} \\ a_p^{m+1} \end{bmatrix}. \quad (32)$$

Matrices  $B$ ,  $D$  and  $G$  are given by

$$B = M + \frac{\Delta t}{Re} K, \quad (33)$$

$$D = \begin{bmatrix} D_s & 0 \\ 0 & D_z \end{bmatrix}, \quad (34)$$

$$G = \begin{bmatrix} G_s & 0 \\ 0 & G_z \end{bmatrix}, \quad (35)$$

where matrices  $M$  and  $K$  are

$$M = \begin{bmatrix} M_s & 0 \\ 0 & M_z \end{bmatrix}, \quad (36)$$

$$K = \begin{bmatrix} 2K_{ss} & K_{zs} \\ K_{sz} & 2K_{zz} \end{bmatrix}. \quad (37)$$

Velocity and pressure fields are decoupled by the Projection Method [10]. The linear systems are solved by PCG (Preconditioned Conjugate Gradient) for velocity and concentration fields and GMRes (Generalized Minimum Residual) for pressure field, employing PETSc library [11].

## 5 CODE VALIDATION

To validate the model and the code, an experimental simulation of a density current problem [4] was carried out, since this is essentially a 2d flow. A flume (450 cm long, 30 cm high and 33 cm wide) was filled (up to 25 cm high) with two fluids of different densities  $\rho$  (see Fig. 7): one half with a solution of salt in water ( $\rho = 1020 \text{ kg/m}^3$ ) and the other with water ( $\rho = 980 \text{ kg/m}^3$ ). The heavier fluid also received an amount of potassium permanganate ( $\text{KMnO}_4$ ) as tracer. The two fluids were initially separated by a vertical wall, when the wall was suddenly removed, allowing the two fluids to mix. Figure 8 shows synchronized frames of the mixing process, experimental and numerical, taken at times  $t = 2, 3, 5, 7, 9, 12, 15$  and  $17$  s.

The simulation showed good timing results. The mixing profile can be improved by mesh refinement, since each code run took approximately 20 minutes to attain time  $t = 17$  s.



**Figure 7** – A picture of the flume used in the experiment.

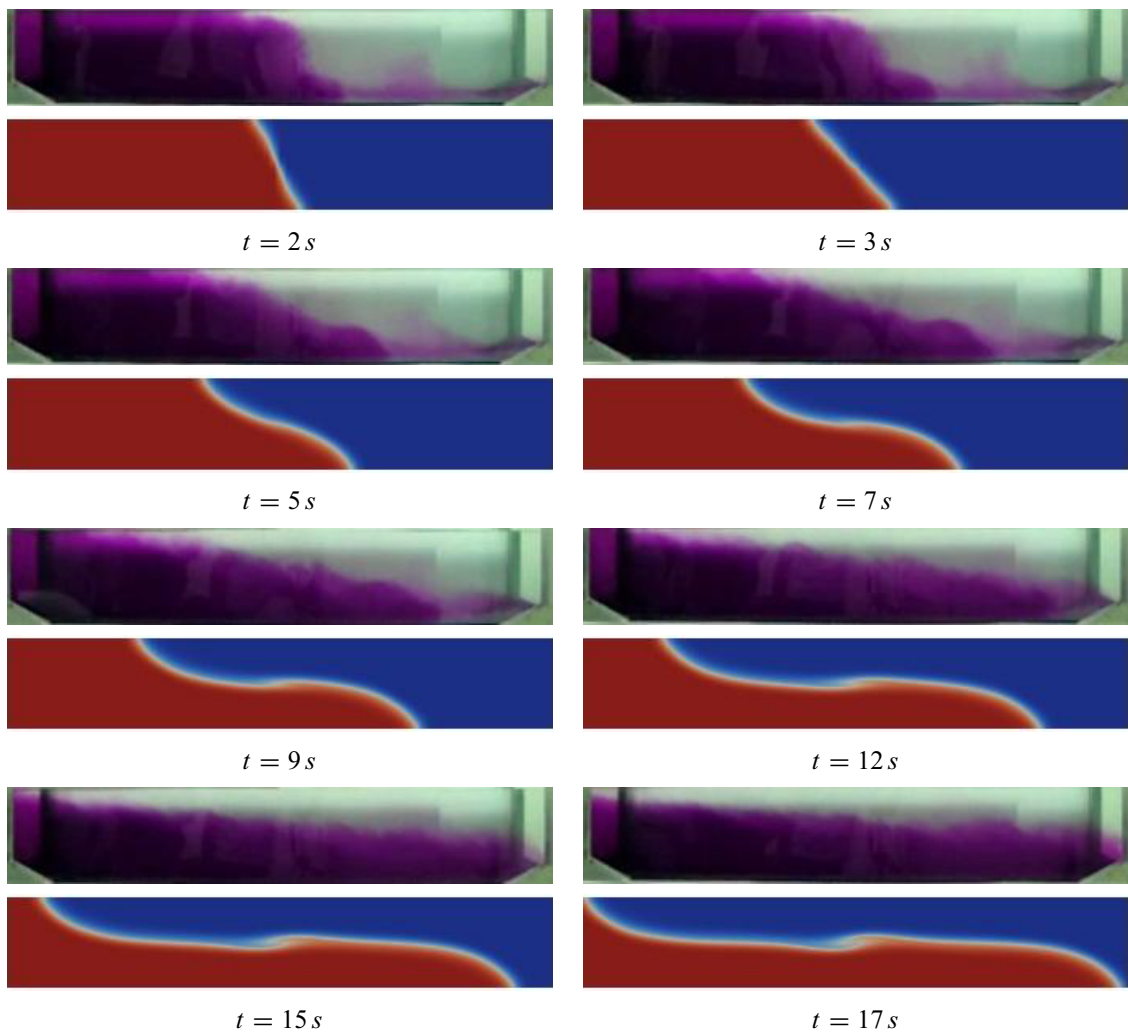


**Figure 8** – Validation of the numerical model represented by Eqs. 26 to 29 and the FEM code employed for solving these equations. The figure presents a comparison between the experimental result of mixing of two fluids with different densities in the flume shown in Figure 7 and the respective numerical result. At each time, the upper frame is a picture taken in the actual flume and the lower one is the numerical result, at the same time. The two fluids are initially separated by a vertical wall at the middle of the flume length. The wall is removed, allowing the mixing of the two fluid.

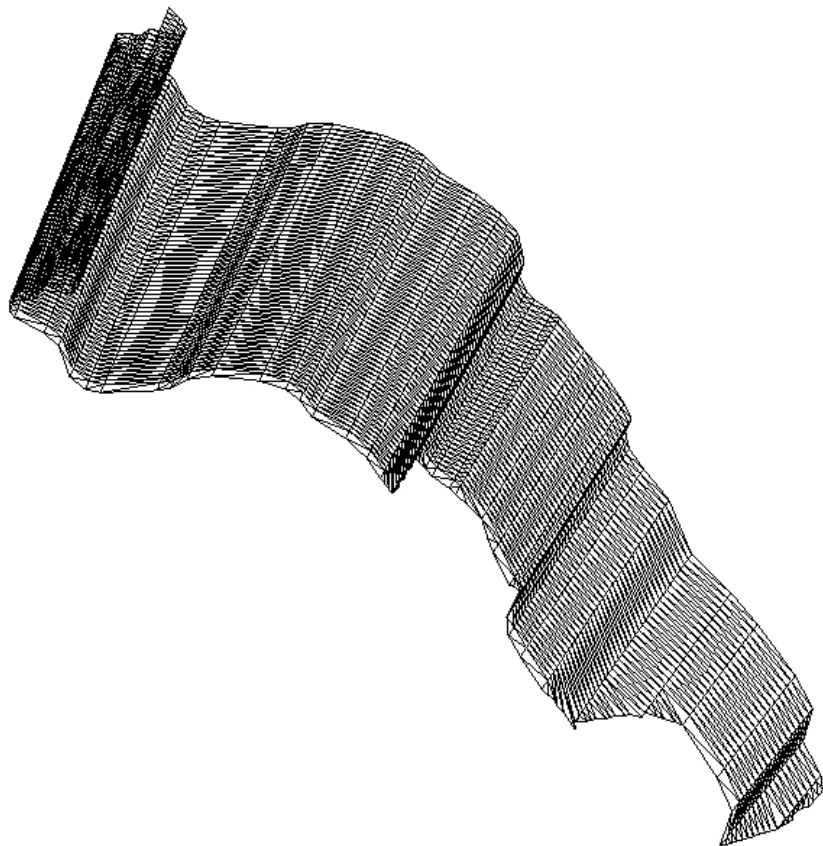


**Figure 9** – Perspective view of 2db mesh.



**Figure 10** – Breadths along the domain.

## 6 RESERVOIR SIMULATION

In this section, numerical results of a reservoir simulation are presented. Water inflow carries a certain solute concentration into the reservoir, with 1 m/s as inflow velocity. The solute inflow concentration value ( $1 \text{ kg/m}^3$ ) was chosen so that strong gravity currents could develop close to the lower surface of the reservoir. The reservoir longitudinal length is 5,962 m, with 800 m of depth, and is discretized in a mesh with 1,503 vertices and 2,736 elements, as shown in Figure 9.

The reservoir breadth is plotted in Figure 10.

The platform for the simulations was a two 1.60GHz Intel Xeon processors computer with 16GB of RAM. Simulation of 2 hours and 38 minutes of real time flow took about 20 CPU minutes. Figures 11.a to 11.d show the solution of the concentration and velocity fields at four different times  $t$ . The vertical mesh simulation is presented in the longitudinal-vertical plane.

Note that, despite the larger density, part of the income concentration flows close to the surface, as an effect of the breadth. Other portion of the income falls to the bottom, forming a vortex in the scale of the reservoir depth.

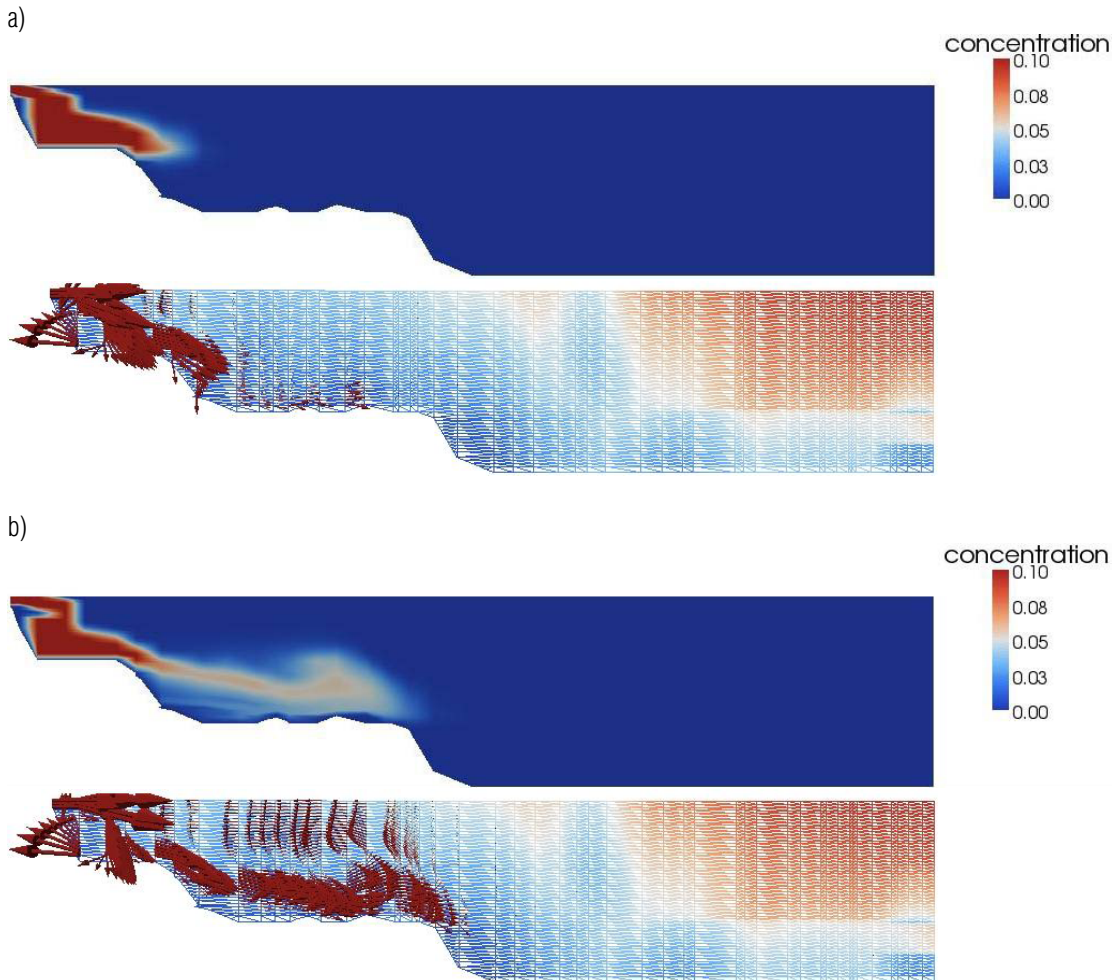


**Figure 11** – (a)  $t = 39$  min; (b)  $t = 1h20min$ .

## 7 CONCLUSION

Computational code tests and experimental validation have shown that the model is capable to simulate important depth dependent environmental flows. Additionally, the 2d approach has proved to be an efficient strategy concerning simulated time per processing time. The low computational cost allows the use of very fine meshes, enhancing the quality of numerical results. The laterally averaged model (2db) and depth averaged model (2dh)—widely used in shallow water simulations [5]—are complementary models, which means that one can obtain satisfactory information by combining 2db and 2dh simulations, without the computational penalty of a heavy 3D simulation. The tool presented in this paper also counts with a complete GUI (Graphical User Interface), where the user can manipulate all terrain, hydrographic and mesh data, making the simulation set up easier.

## ACKNOWLEDGMENTS

We thank Promon Engenharia and FURNAS Centrais Elétricas for financial and technical support and CNPq and FAPERJ for financial support.

## REFERENCES

- [1] DONGALA AM, LIMA LMR, MANGIAVACCHI N & SOARES CBP. 2006. Finite element mesh generation for numerical simulation of hydroelectric power plant reservoir filling. Proceedings of the 11<sup>th</sup> Brazilian Congress of Thermal Sciences and Engineering, Curitiba, Brazil, pp. 41–44.
- [2] JORGENSEN SE. 1979. Handbook of Environmental and Ecological Parameters, Pergamon Press, Oxford.
- [3] KARPIK SR & RAITHBY GD. 1990. Laterally Averaged Hydrodynamics Model for Reservoir Predictions. Journal of Hydraulic Engineering, 116: 6.

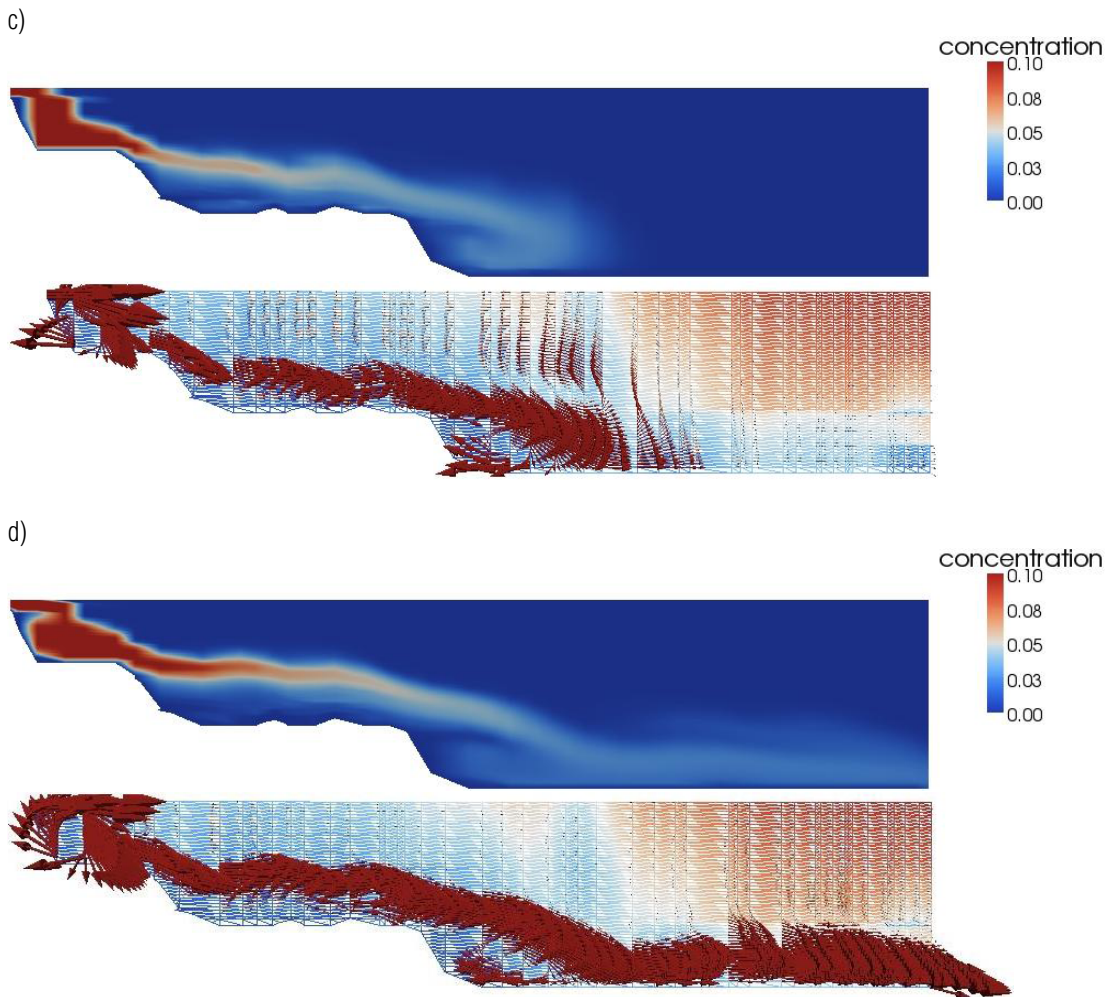


**Figure 11 – (c)  $t = 1\text{h}58\text{min}$ ; (d)  $t = 2\text{h}38\text{min}$ .**

- [4] PATERSON MD, SIMPSON JE, DALZIEL SB & NIKIFORAKIS N. 2005. Numerical Modeling of Two-dimensional and Axissymmetric Gravity Currents. *International Journal for Numerical Methods in Fluids*, 47: 1221–1227.
- [5] ROSMAN PCC. 2001. Um Sistema Computacional de Hidrodinâmica Ambiental. In: SILVA RCV. *Métodos Numéricos em Recursos Hídricos 5.1*, Ed. Porto Alegre: ABRH, 5: 1–161.
- [6] CAREY GF. 1995. *Finite Element Modeling of Environmental Problems*, John Wiley & Sons, England.
- [7] DONGALA AM, LIMA LMR, MANGIAVACCHI N & SOARES CBP. 2007. Organic Matter Decay Modeling for Numerical Simulations of Hydroelectric Reservoir Filling. *Proceedings of the 19<sup>th</sup> International Congress of Mechanical Engineering – COBEM*, Brasília, Brasil.
- [8] SOARES CBP. 2003. Modelagem e Simulação de Sistemas Aquáticos em Ambiente de Geoprocessamento, DSc Thesis, Federal University of Rio de Janeiro.
- [9] ALDRIGHETTI E. 2007. Computational Hydraulic Techniques for the Saint Venant Equations in Arbitrarily Shaped Geometry, PhD Thesis, Università Degli Studi di Trento.
- [10] DENARO FM. 2003. On the Application of the Helmholtz-Hodge Decomposition in Projection Methods for Incompressible Flows with General Boundary Conditions. *International Journal for Numerical Methods In Fluids*, 43: 43–69.
- [11] TORRES P & MANGIAVACCHI N. 2010. Parallel Numerical Simulations of Water Reservoir. *AIP Conf. Proc.* 1301, pp. 446–454; doi: <<http://dx.doi.org/10.1063/1.3526644>> (9 pages). *Application of Mathematics in Technical and Natural Sciences: Proceedings of the 2<sup>nd</sup> International Conference – Sozopol*, Bulgaria.